Renewable and Sustainable Energy Reviews 31 (2014) 554–562

Contents lists available at ScienceDirect

Renewable and Sustainable Energy Reviews

journal homepage: www.elsevier.com/locate/rser

Designing building envelope with PCM wallboards: Design tool development

Arash Bastani [a], Fariborz Haghighat [a,*], Janusz Kozinski [b]

[a] Department Building, Civil and Environmental Engineering, Concordia University, Montreal, QC, Canada H3G 1M8
[b] Lassonde School of Engineering, York University, Toronto, ON, Canada

ARTICLE INFO

Article history:
Received 2 April 2013
Received in revised form
15 November 2013
Accepted 18 December 2013
Available online 21 January 2014

Keywords:
Phase change materials
Building envelope
Design
Thermal energy storage
Buildings

ABSTRACT

While space conditioning load contributes largely in grid critical peak, shifting a part or full to the off-peak period could have significant economic effects on both energy supply and demand sides. This shifting technique is accomplished by storing energy during off-peak periods to be utilized during peak periods. The wallboard enhanced with PCM can provide latent heat thermal energy storage (TES) distributed in the whole surface area of the building envelope and evade the enhanced thermal mass in light weight buildings. Identifying the best design parameters of the PCM wallboard is the main key to apply this latent heat TES efficiently.

The effective dimensionless numbers on the thermal dynamics of a PCM wallboard were identified. Moreover, the impact of the change of those numbers on the time required for the wallboard to become fully charged was evaluated. This parametric study provided a tool to characterize the required thickness of a PCM wallboard which needs to be charged during the off-peak. The tool presents the Fourier number as a correlation of Biot number and Stefan number. Moreover, the impact of melting range on the charging time of a PCM wallboard was investigated.

Contents

1. Introduction

Building sector contributes largely in total energy consumption, particularly for its space conditioning. According to The Natural Resources CANADA [26], while more than 30% of the total secondary energy was used by residential and commercial/institutional buildings, space heating accounts up to 56% of the total energy used in non-industrial buildings. In Quebec, Canada, 70% of residential buildings use electrical space heating system which accounts for 29% of the grid critical peak [9]. Its total usage varies during a day due to the activities of industrial, commercial, and residential sectors together. This results in peak period (mostly in early morning and evening) and off-peak periods. According to HydroQuebec [10], during the peak period in winter the electricity cost to the utility company is 10 $/kW to generate and could increase up to 40 $/kW in 2015. Taking this information into account, shifting a significant portion or the whole required energy for space heating to off-peak periods would have significant economic effects on both energy supply and demand. The shifting can be accomplished by storing energy during off-peak periods to be utilized during peak periods. Building envelope and central thermal storage have been used as thermal energy storage (TES). Recently, TES has attracted increasing attention due to the potential benefits it can offer in energy efficiency, in shifting load from

* Corresponding author. Tel.: +1 514 848 2424; fax: +1 514 848 7965.
E-mail address: Fariborz.Haghighat@concordia.ca (F. Haghighat).

1364-0321/$ - see front matter
http://dx.doi.org/10.1016/j.rser.2013.12.031

Nomenclature

T	temperature [°C]
ΔT	melting range [°C]
ρ	density [kg m^{-3}]
Cp	specific heat capacity [J kg^{-1} K^{-1}]
t	time [s]
k	conductivity [W m^{-1} K^{-1}]
x	space coordinate [m]
f	liquid fraction
L	latent heat [J kg^{-1}]
α	thermal diffusivity [m^2 s]
h	heat transfer film coefficient [W m^{-2} K^{-1}]
l	wallboard thickness [m]

Dimensionless parameters

X	dimensionless space coordinate
θ	dimensionless temperature
Fo	Fourier number
Ste	Stefan number
Bi	Biot number

Subscript

f	fusion
s	solid/solidification
l	liquid
m	melting
in	indoor
pc	PCM
Low.Op.Temp.	the lowest operating temperature
High.Op.Temp.	the highest operating temperature

Abbreviation

TES	thermal energy storage
PCM	phase change material
DSC	differential scanning calorimeter

peak to off-peak, in emergency heating/cooling load, in economics and in environmental impact [2,5,18,24]. Moreover, TES is known as an essential mean in designing net zero energy buildings (NZEB) [25]. TES has a significant role in remitting the mismatch between the energy demand time and renewable energy production time. Advanced design tools and technical improvements are required in TES technologies and systems. Indeed the design of the building and TES are often not coordinated. A building integrated with distributed thermal storage materials could shift most of peak load to off-peak time period.

Previous studies investigated the possibility of the peak-load shifting by storing the sensible heat in building materials [3,15,16]. Moreover, the application of phase change materials (PCMs) as a latent heat thermal storage draws interests as a TES with higher capacity. The application of PCM as a TES in buildings was reviewed in details by previous researchers [4,8,12,14,17–19,22,27,29,30]. One promising way to improve the thermal inertia of a building is to integrate PCM layers in its envelope. Due to considerably large area of the envelope of a building, integrating PCM in the envelope can provide a TES with a large capacity. Regular building wallboard can be a mean to accommodate PCMs. The wallboard enhanced with PCM can provide latent heat TES distributed in the whole surface area of the building shell and evade the enhanced thermal mass in light weight buildings. The design parameters of a PCM wallboard consists of its thickness and thermo-physical properties, directly impact the thermal dynamics of the TES and consequently the temperature profile and the space condition enclosed by the wallboards. Identifying the best design parameters of the PCM wallboard is the main key to apply this latent heat TES efficiently. The design parameters of the wallboard depend on its application and require the knowledge of the influence of those parameters on the thermal dynamics of the PCM wallboard. Reviewing previous studies presents some achievements regarding the best design of a PCM wallboard. Neeper [23] investigated the optimum melting temperature and melting range of a gypsum wallboard impregnated with fatty acid and paraffin waxes in a passive design. He, also, conducted the study for two different magnitudes of the convective heat transfer coefficient between a wallboard to the room. He concluded that the optimum melting temperature depends on the outdoor seasonal conditions and the average room temperature. He, also, suggested a melting temperature equal to the room average temperature with a narrow phase change temperature range (around 2°). Kuznik et al. [13] investigated the effect of insulation thickness, indoor temperature and outdoor temperature swing on the optimum thickness of an encapsulated PCM wallboard. The objective of the optimization was to maximize the energy storage capacity with the smallest PCM thickness. Their results showed that the variation of the outdoor temperature swing and insulation thickness does not affect the optimum design thickness of the PCM layer. However, increasing the indoor temperature swing resulted in an increase in the optimum design thickness of the PCM wallboard. Ahmad et al. [1] reported that the PCM thermo-physical properties impact the thermal dynamics of the PCM layer and consequently the building thermal performance. Lin et al. [20] studied the effect of the thickness, conductivity, melting temperature and the latent heat of a shape-stabilized PCM on the room air temperature profile. Xu et al. [28] concluded that there is minimum thickness of the PCM layer, and suggested that the conductivity and latent heat of the PCM should be more than 0.5 [W m^{-1} K^{-1}] and 120 [kJ kg^{-1}], respectively. Overall, the outcomes of the abovementioned studies emphasize that the best design parameters depends on the design objectives, and the environmental conditions. Although those works brought some general suggestions for the application of a PCM in building envelope, the results are inherently case specific and cannot be generalized for the design of an integrated building envelope with PCM. A procedure to generalize the results, specifically for numerical studies, is to conduct the simulation and parametric studies using dimensionless numbers. Ettouney et al. [6,7] characterizing the heat transfer process in PCM applied in double pipe and spherical storage. They provided some correlations for the melting and solidification: Fourier number (Fo) as a function of the Stefan number (Ste) and Biot number (Bi) of the PCM. Those dimensionless numbers content the thickness, heat transfer coefficients and the thermo-physical properties of the materials. Therefore, any possible change of the characteristics of the materials, which affects the thermal storage/release process inside the PCM, can be evaluated deploying the correlation available between those dimensionless numbers. Yet, the lack of similar correlations for PCM wallboards requires extended studies on the application of these materials in building envelope. The aim of this study is to investigating the application of PCM wallboard inside the building envelope to be able to shift the peak load for space conditioning to the off-peak period. Indeed, the interest is to store energy during the off-peak period for space conditioning during the peak period, to evade the application of spacing heating/cooling systems at those peak hours. For this purpose,

the PCM wallboards need to be evaluated based on their characteristics in a way to determine the required time to be charged. Therefore, the main objective of this study is to develop a procedure to design a PCM wallboard for a given application.

2. Methodology and problem formulation

To obtain the best design parameters of a PCM wallboard, characterizing the impact of the design parameters on its thermal performance is required. Generally, the influential parameters are the ones which affect the heat transfer rate through the wallboard and the storage capacity. Therefore, the thermo-physical properties of the PCM wallboard, its thickness, and convective heat transfer coefficient characterize its thermal performance. To investigate the impact of these parameters, recognizing the effective dimensionless numbers for such physical phenomenon is required. Characterizing the impact of these dimensionless numbers concludes the correlations between these numbers and the performance of PCM wallboards. Numerical simulation is deployed to characterize the thermal performance of a PCM wallboard.

The main difficulty in modeling a PCM is the process of melting and/or solidification state. When the temperature of the PCM reaches its melting temperature range, the material is gradually changing from one phase to another one. Considering T_f [°C] as the fusion temperature of PCM, generally the material transits from one state to another one in a range of temperature (ΔT) around its fusion temperature. Herein, when the temperature of the material is less than the lower bound of the melting range (solidification temperature T_s), the material is completely solid. Also, when the temperature of the material is higher than the upper bound of the melting range (melting temperature T_m), the material is completely liquid. When the temperature of the material is in the melting range, both solid and liquid states coexist together. The part of the material which both solid and liquid coexist together is called mushy zone. Characterizing the thermo-physical properties of a pure PCM or a composite of PCM and building material, i.e. wallboard with encapsulated PCM, is required to simulate the phase-change phenomenon in a PCM wallboard. Differential scanning calorimeter (DSC) is a well known method to characterize the heat of fusion, fusion temperature, melting range, and specific heat capacity of the material as a function of temperature. Generally, a wallboard composed of PCM and regular building material is analyzed through DSC analysis yields to identifying its thermo-physical properties and specific heat capacity as a function of temperature.

Neglecting convective heat transfer inside the liquid zone, heat transfer inside the PCM wallboard can be characterized using heat equation modified by adding a term to govern the absorption and release of latent heat during the phase transition as follow:

$$\rho C_p \frac{\partial T}{\partial t} = k_{s/l} \frac{\partial^2 T}{\partial x^2} + S \tag{1}$$

Here, ρ is the density [kg m^{-3}], Cp is the heat capacity [J kg^{-1} K^{-1}], T is the temperature [K], t is the time [s], $k_{s/l}$ is the conductivity in solid/liquid [W m^{-1} K^{-1}], and the term S is introduced to account for the source/sink of latent heat. It is presented as:

$$S = \rho L \frac{\partial f}{\partial t} \tag{2}$$

This equation implies that the rate of absorption and release of latent heat depend on the rate of change of the liquid fraction. By using the chain rule, Eq. (2) is reconfigured as:

$$S = \rho L \frac{\partial f}{\partial T} \frac{\partial T}{\partial t} \tag{3}$$

where the L is the PCM latent heat [J kg^{-1}]. Liquid fraction is assumed to be changed linearly between solidification temperature and melting temperature. Thus, the liquid fraction as a function of time is:

$$f(T) = \frac{T - T_s}{T_m - T_s} \tag{4}$$

where T_s is the solidification temperature and T_m is the melting temperature. In this study, the lower bound and upper bound of the melting range are called solidification temperature and melting temperature, respectively.

The PCM wallboard temperature, and consequently its liquid fraction have three states:

$$f(T) = \begin{cases} 0 & T < T_s \quad \textit{Solid} \quad \frac{\partial f}{\partial T} = 0 \\ ]0,1[& T_s < T < T_m \quad \textit{Mushy} \quad \frac{\partial f}{\partial T} \neq 0 \\ 1 & T > T_m \quad \textit{Liquid} \quad \frac{\partial f}{\partial T} = 0 \end{cases} \tag{5}$$

To have the non-dimensional format of Eq. (1), the following dimensionless parameters were taken into account;

$$X = \frac{x}{l}$$

$$\text{Dimensionless PCM temperature} : \theta_{PC} = \frac{T - T_s}{T_m - T_s}$$

$$\text{Fourier number} : F_o = \frac{\alpha t}{l^2}$$

$$\text{Stefan number} = \text{Ste} = \frac{C_p \Delta T}{L} \quad (\text{where } \Delta T = 1\ ^\circ\text{C})$$

where l is the thickness of PCM wallboard, and α is the thermal diffusivity. Regarding the definition of the Stefan number as the ratio of sensible heat over the latent heat, ΔT is assumed to be 1 °C. Therefore, the antecedent of the ratio in Stefan number is the sensible heat stored in a unit of mass of a material when its temperature increases by 1 °C.

By replacing Eq. (3) in Eq. (1);

$$\rho C_p \frac{\partial T}{\partial t} = k \frac{\partial^2 T}{\partial x^2} + \rho L \frac{\partial f}{\partial T} \frac{\partial T}{\partial t} \tag{6}$$

Replacing the dimensionless parameters in Eq. (6), it is rearranged as;

$$\left(1 - \frac{\Psi}{Ste} \frac{\partial f}{\partial \theta_{PC}}\right) \frac{\partial \theta_{PC}}{\partial F_o} = \frac{\partial^2 \theta_{PC}}{\partial X^2} \tag{7}$$

where,

$$\frac{1\ ^\circ C}{(T_m - T_s)} = \text{constant} = \Psi \tag{8}$$

The boundary condition is non-dimensionlised as follow;

$$k \frac{\partial T(0,t)}{\partial x} = h(T_{in} - T(0,t)) \tag{9}$$

where T_{in} is the room temperature and h is the heat transfer coefficient which consists of both convection heat transfer coefficient and long wave radiation heat transfer coefficient. To study the effect of indoor operation temperature, a secondary dimensionless temperature is also introduced as follow;

$$\theta_{in} = \frac{T_{in} - T_{low\ Op.Temp.}}{T_{High\ op.Temp.} - T_{Low\ Op.Temp.}} \tag{10}$$

where T_{in} is the indoor temperature, $T_{Low\ Op.Temp.}$ and $T_{High.\ Op.Temp.}$ are the lowest and the highest operating room air temperatures, respectively. Considering these two operating temperatures,

solidification temperature, and melting temperature, the following constants dimensionless values can be expressed as;

$$\Psi_{op} = \frac{T_{High\ Op.Temp.} - T_{Low\ Op.Temp.}}{T_m - T_s} \tag{11}$$

$$\Psi_{PC} = \frac{T_s - T_{Low\ Op.Temp.}}{T_m - T_s} \tag{12}$$

These two constant values show the relation between the melting range and the indoor operating temperatures. Using those dimensionless parameters, Eq. (9) is modified as follow;

$$\frac{\partial \theta_{PC}(0,t)}{\partial X} = Bi\{[\theta_{in}(t)\Psi_{Op} + \Psi_{PC}] - \theta_{PC}(0,t)\} \tag{13}$$

Based on those equations, the thermal performance of a PCM wallboard is defined as;

$$\theta_{PC} = f(Bi, Fo, X, Ste, \Psi, \Psi_{Opt}, \Psi_{PC}) \tag{14}$$

These non-dimension parameters are used to conduct the parametric studies to find the effect of design parameters on the performance of the PCM wallboard. Moreover, the possible correlations between those parameters are practical tools for designing PCM wallboards.

2.1. Numerical method

To simulate the heat transfer through a PCM wallboard, Eq. (1) was solved numerically using finite difference technique. The Crank–Nicolson implicit numerical scheme is adopted to solve the parabolic partial differential heat equation. For the node i in the time step n, the equation becomes:

$$-(r_i^n)T_{i-1}^{n+1} + 2(1+r_i^n)T_i^{n+1} - (r_i^n)T_{i+1}^{n+1} = (r_i^n)T_{i-1}^n + 2(1-r_i^n)T_i^n + r_i^n T_{i+1}^n \tag{15}$$

where;

$$r_i^n = \frac{k_i^{n-1}\Delta t}{\Delta x^2 \rho (C_p + Lf')} \tag{16}$$

and,

$$f' = \frac{f_i^{n-1} - f_i^{n-2}}{T_i^{n-1} - T_i^{n-2}} \tag{17}$$

First and second order partial derivatives are selected in terms of central differences for internal nodes, while at boundaries the forward and backward differences were applied with second order approximation. MATLAB [21] was used to solve the system of equation.

Before conducting the parametric study, the PCM model was validated with the benchmark (task C) defined by ANNEX 23 [11]. The task consists of a number of PCM wallboard configuration cases for simulation. The cases assumed no short wave radiation. Here, he model was validated with one case (P10) which investigates the temperature distribution inside a 10 mm PCM wallboard. The parameters of the PCM and the specifications of the simulated case are presented in Table 1. Fig. 1 shows the interior and exterior surface-temperatures of the PCM wallboard and it shows that there is a good agreement between two results. Moreover, Fig. 2 presents the liquid fraction along the wallboard in different time; the phase transition phenomenon in PCM wallboard. Based on the liquid fraction magnitude, liquid zone, mushy zone and solid zone can be distinguished along the wallboard.

Table 1
The parameters of the PCM and the boundary conditions of Task C ANNEX 23 [11].

The parameters of the PCM and boundary conditions	Task C ANNEX 23
Wallboard thickness [m]	0.01
Conductivity [W m^{-1} K^{-1}]	0.25 $T<23$ °C
	0.20 $T>23$ °C
Density [kg m^{-3}]	1100
Specific heat [J kg^{-1} K^{-1}]	2500
Latent heat [J kg^{-1}]	71,000
Solidification temperature [°C]	14
Melting temperature [°C]	28
Inside convection heat transfer coefficient [W m^{-2} K^{-1}]	2.5
Outside convection heat transfer coefficient [W m^{-2} K^{-1}]	8
Inside air temperature [°C]	20
Outside air temperature [°C]	$12+10\times t$ $t<2$ h
	32 $t>2$ h
Initial condition [°C]	12

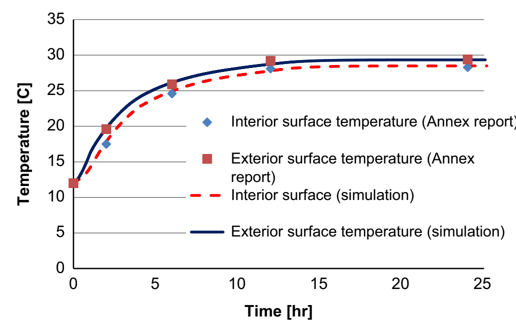


Fig. 1. Validation of the PCM model with Case P10 in task C of Annex 23 [11].

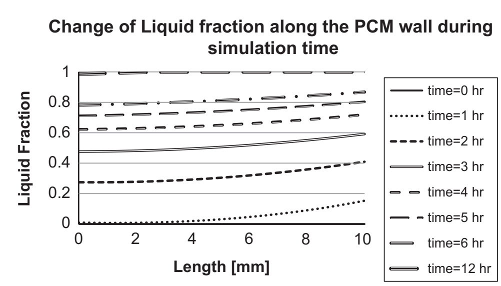


Fig. 2. Change of liquid fraction along the PCM wallboard with time.

3. Results and discussions

3.1. Simulation scenario

To simulate the thermal performance of a PCM wallboard, it is assumed that the layer is mounted as the interior layer of a wall section. Thus, the PCM has room temperature as its boundary condition in one side, and adiabatic boundary condition on the other side (prefect insulation or similar room air condition on the other side). This assumption is valid for internal walls which are utilized as partition or separating two zones with the same thermal conditions, and the external walls of well insulated building. Effective insulation with very low thermal conductivity creates almost no heat flux boundary condition for the interior layer which has the potential to be replaced by PCM layer. Fig. 3 illustrates the schematic diagram of a mounted PCM layer in an external wall section.

The room temperature is assumed to be equal to the set point temperature. Therefore, the sudden increase or decrease of the set-point temperature results in the consecutive change of the room temperature. Here, to charge the PCM wallboard, the set-point

temperature is increased from the lower bound of the thermal comfort to its upper bound. Thus, the wall which is conditioned in the room temperature faces with a temperature solicitation on its boundary. The time requires charging the PCM depends on the design parameters of the PCM wallboard. These design parameters are film coefficient and the PCM's thickness, thermal conductivity, heat capacity, and the latent heat, which can be summarized as the *Ste* and *Bi* number of the PCM layer. Moreover, the *Fo* number gives a measure of charging/discharging time.

To investigate the effect of *Ste* number on the performance of a PCM layer, a number of simulations were conducted with different *Ste* numbers while the *Bi* number was kept constant at 0.4. It was assumed that both the wall and the room initial temperature was 20 °C, and the phase transition occurred between 17 and 23 °C. The set-point temperature and consequently the room temperature were suddenly increased to 25 °C to evaluate the time required to charge the PCM wallboard. Ten different cases with various *Ste* were designed and simulated. To generate different *Ste* number, both heat capacity and latent heat were altered. The information of the simulated cases is tabulated in Table 2. Moreover, the inner surface temperature profile of the PCM wallboard is presented in Fig. 4.

Fig. 4 shows that the temperature profile has two separate trends. At first the wall has both latent and sensible heat storage. When the PCM is completely liquefied, then there is only sensible heat storage and the trend of the temperature profile is changing. Comparing the former state of storage with the lateral one, the change of θ_{pc} occurs in a larger Fourier number when both sensible and latent heat storage coexist together.

Three specific Fourier numbers were calculated for each case base on the wall thermal situation; (1) when half of the PCM is fully liquefied, (2) when the whole PCM is fully liquefied, and (3) when the wall gets to steady state condition (no more change in temperature at 25 °C). As illustrated in Fig. 5, the change of those *Fo* numbers versus *Ste* number of the PCM wallboard were linear with an almost similar slope of 0.42. Also as presented in Table 2, both case 6 and case 7 have $Ste^{-1}=50$, while they have different heat capacity and latent heat. However, in both cases, all those measured *Fo* were almost the same.

To investigate the correlation of *Fo* number versus *Ste* number, the study was conducted for different *Bi* number and *Ste* numbers. The PCM parameters in these simulation cases are presented in Table 3.

Fig. 6 shows variation of *Fo* as a function of *Ste* number and *Bi* numbers for both completely liquefied time and steady state condition of the PCM wallboard.

Fig. 6a and b shows that the change of *Fo* as a function of $(Ste)^{-1}$ number is linear for a given *Bi* number. While the slope of the graphs is the same for both fully liquefied and steady state *Fo* numbers for a given *Bi* number. It also shows that the magnitude of the slope varies when the *Bi* number is changed.

Fig. 7 shows the change of *Fo* as a function of *Bi* number for different *Ste* number for both completely liquefied PCM and steady state condition. Here, unlike the correlation for the *Ste* number,

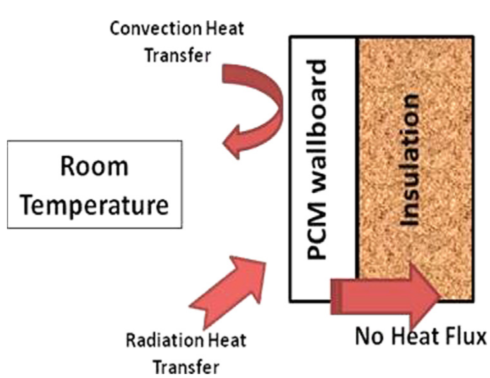


Fig. 3. Schematic diagram of a PCM wallboard in the simulation scenario in an external wall section.

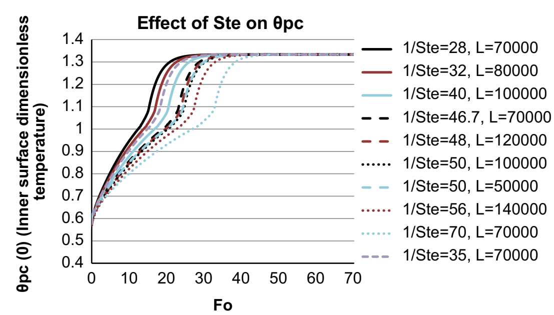


Fig. 4. The change of inner surface temperature (θ_{pc}) VS *Fo* for different *Ste* number.

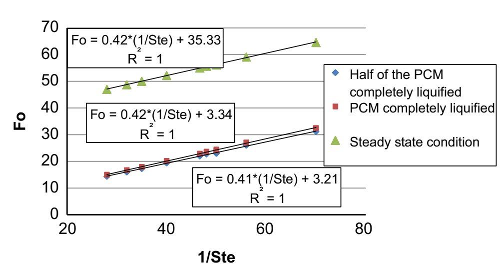


Fig. 5. Variation *Fo* vs $(Ste)^{-1}$ for $Bi=0.4$.

Table 2
Simulation cases for various *Ste* number.

Case	Heat Capacity (*Cp*) [J kg^{-1} K^{-1}]	Latent (*L*) [J kg^{-1}]	Ste^{-1}	*Bi*	*Fo* (half of the PCM completely liquefied)	*Fo* (PCM completely liquefied)	*Fo* (steady state condition)
Case 1	2500	70,000	28.00	0.4	14.36	15.00	47.00
Case 2	2500	80,000	32.00	0.4	16.00	16.73	48.73
Case 3	2500	100,000	40.00	0.4	19.36	20.18	52.18
Case 4	1500	70,000	46.67	0.4	21.97	22.88	55.00
Case 5	2500	120,000	48.00	0.4	22.73	23.64	55.64
Case 6	2000	100,000	50.00	0.4	23.41	24.43	56.48
Case 7	1000	50,000	50.00	0.4	22.95	24.09	56.14
Case 8	2500	140,000	56.00	0.4	26.00	27.09	59.09
Case 9	1000	70,000	70.00	0.4	31.14	32.50	64.54
Case 10	2000	70,000	35.00	0.4	17.27	17.95	50.00

In all cases: thickness l=0.01 m, conductivity $k=0.25$ [W m^{-1} K^{-1}], density $\rho=1100$ [kg m^{-3}], and melting range [17–23 °C].

Table 3
Simulation cases for different *Bi* and *Ste*.

Case	Thickness [m]	Heat capacity(Cp) [J kg^{-1} K^{-1}]	Conductivity (k) [W m^{-1} K^{-1}]	Latent heat (L) [J kg^{-1}]	$(Ste)^{-1}$	*Bi*	[a]*Fo*	[b]*Fo*	[c]*Fo*
Case 11	0.010	2500	0.50	75,000	30	0.2	28.73	29.45	89.64
Case 12	0.014	1000	0.70	50,000	50	0.2	44.16	45.13	106.17
Case 13	0.006	1500	0.30	105,000	70	0.2	58.58	60.10	120.20
Case 14	0.011	2700	0.15	81,000	30	0.7	9.39	10.03	30.00
Case 15	0.025	900	0.35	45,000	50	0.7	14.49	15.43	35.40
Case 16	0.018	1700	0.25	119,000	70	0.7	19.69	20.91	40.82
Case 17	0.030	2000	0.75	60,000	30	0.4	15.30	15.91	47.92
Case 9	0.010	2000	0.25	100,000	50	0.4	23.41	24.43	56.48
Case 6	0.010	1000	0.25	70,000	70	0.4	31.14	32.50	64.54

In all cases: Density $\rho = 1100$ [kg m^{-3}], melting range [17–23 °C].

[a] Half of the PCM completely liquefied.
[b] PCM completely liquefied.
[c] Steady state condition.

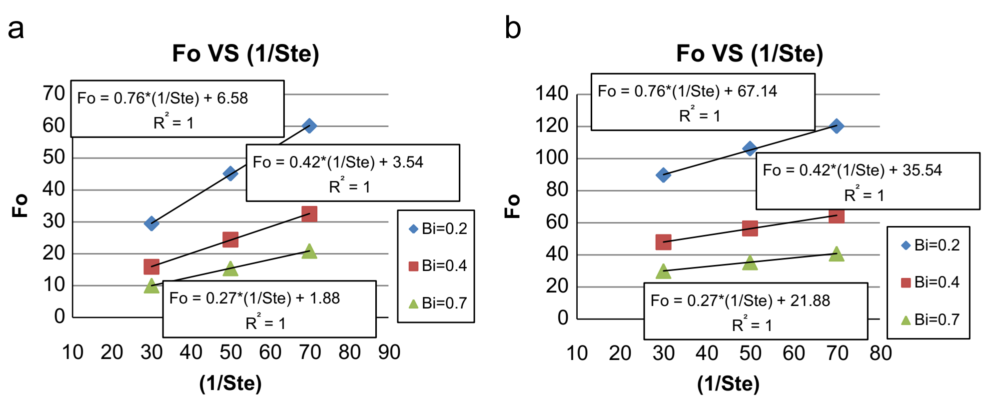


Fig. 6. *Fo* VS $(Ste)^{-1}$ in different *Bi* numbers (a) PCM completely liquefied, (b) steady state condition.

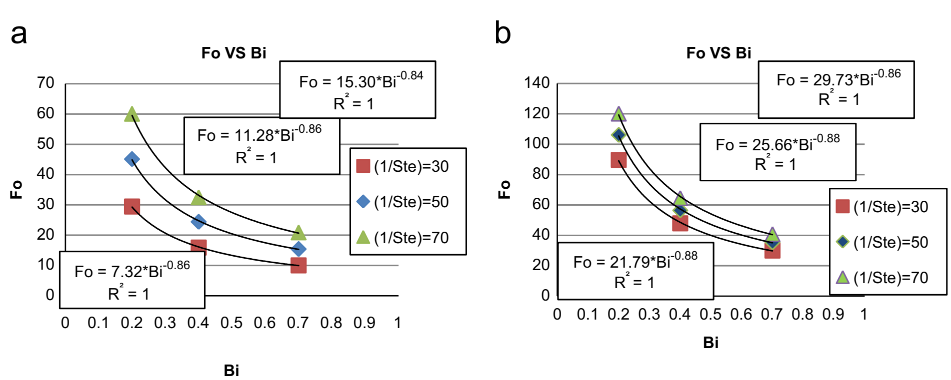


Fig. 7. *Fo* VS *Bi* in different $(Ste)^{-1}$ numbers (a) PCM completely liquefied (b) steady state condition.

Table 4
The specifications of the testing scenarios.

Testing case	Thickness [m]	Heat capacity [J kg^{-1} K^{-1}]	Conductivity [W m^{-1} K^{-1}]	Latent heat [J kg^{-1}]	$(Ste)^{-1}$	*Bi*	[a]*Fo*	[b]*Fo*	Error [%]
Case 1	0.038	1640	0.43	93000	57	0.88	14.54	14.11	2.93
Case 2	0.049	1240	0.93	144000	116	0.53	42.17	41.82	0.82
Case 3	0.008	1360	0.71	84000	62	0.11	92.70	88.75	4.26
Case 4	0.010	2790	1.10	126000	45	0.09	88.17	80.20	9.03
Case 5	0.030	2070	0.35	195000	94	0.86	23.62	22.81	3.43
Case 6	0.021	1940	0.82	370000	191	0.26	126.95	121.58	4.23
Case 7	0.015	2610	0.66	355000	136	0.22	102.38	99.75	2.56
Case 8	0.017	2940	0.50	66000	22	0.33	14.50	15.16	4.53
Case 9	0.012	860	0.88	158000	184	0.14	214.47	199.36	7.04
Case 10	0.025	620	0.52	117000	189	0.49	71.24	71.14	0.13

In all cases: density $\rho = 1100$ [kg m^{-3}], melting range [17–23 °C].

[a] PCM completely liquefied (simulation).
[b] PCM completely liquefied (Fig. 8).

logarithmic magnitude of *Fo* is changing linearly with the logarithmic value of *Bi*. By increasing the *Bi* number the *Fo* of completely liquefied and steady state condition are decreasing. As presented in Fig. 7a, the correlation for different $(Ste)^{-1}$ has almost similar exponent (0.86). The same equality was observed in Fig. 7b for the steady state condition (exponent for all $(Ste)^{-1}$ is around 0.88).

The correlations shown in Figs. 6 and 7 can be used to estimate the time required to fully charge a PCM wallboard. Depending on the applications, the PCM wallboard as the thermal storage needs to be conditioned to a certain temperature in a given period of time. In another word, these correlations can be used as a design tool to find the optimum parameters of a PCM wallboard to store the required thermal storage in a pre-determined time period.

To evaluate the accuracy of the developed tool, ten design scenarios were selected in which the *Fo* of a fully melted PCM was calculated using the correlations developed in this study. Then, the results of those testing scenarios were compared with the *Fo* calculated using mathematical simulation. The thickness and the thermo-physical properties of the PCM wallboards in those testing scenarios were selected randomly for the following ranges; thickness (0.005–0.05 m), heat capacity (500–3000 J kg^{-1} K^{-1}), conductivity (0.1–1.2 W m^{-1} K^{-1}), and latent heat (50,000–400,000 J kg^{-1}).The aforementioned ranges were selected based on the available materials in literatures. The specifications of the PCM wallboard in the testing scenarios are presented in Table 4. Fig. 8 shows the *Fo* for completely liquefied PCM for various *Bi* and *Ste* numbers. Fig. 8 makes it possible to calculate the time required to fully melt a PCM wallboard with melting range of [17–23 °C], when the operation temperature is changing from 20 to 25 °C.

For the testing scenarios, the *Fo* number was calculated using both simulation results and the graph in Fig. 8. To compare the chart with the simulation, the simulation results are presented as the circular markers in Fig. 8. The relative error between both calculation methods was determined. The mean average error for the testing scenarios was less than 4%.

To find the correlation relating *Fo* number of completely liquefied PCM wallboard to its *Bi* and *Ste* numbers, 100 cases with different *Bi* and *Ste* were surface-fitted employing MATLAB

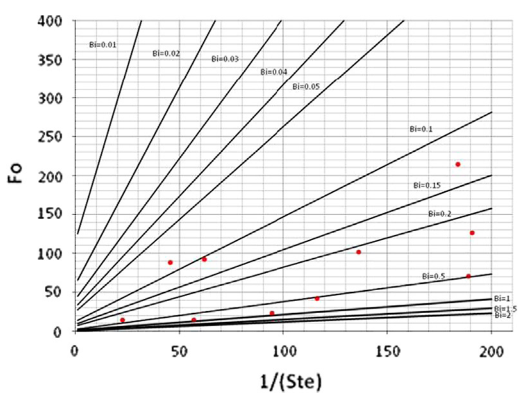


Fig. 8. *Fourier number* of completely liquefied PCM wallboard as function of *Bi* and $(Ste)^{-1}$ numbers.

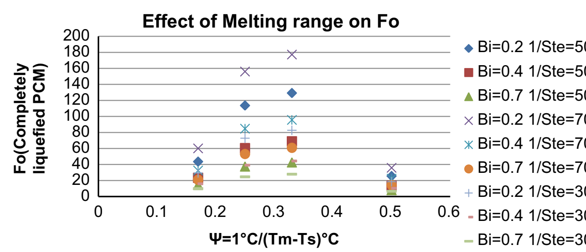


Fig. 10. Effect of melting range on *Fo* measured for completely liquefied PCM.

Table 5
Scenarios with different melting range.

PCM wallboard parameters		*Fo* of completely liquefied in Ψ equal to				Fitted Gaussian function			
Bi	Ste^{-1}	0.17	0.33	0.50	0.25	*a*	*b*	*c*	*r*-square
0.2	50	43.64	129.22	25.65	113.64	133.70	0.31	0.14	0.99
0.4	50	23.41	68.98	13.52	60.45	71.31	0.31	0.14	0.99
0.7	50	14.49	42.64	8.01	37.52	44.16	0.31	0.14	1.00
0.2	70	60.10	177.27	35.86	156.06	183.5	0.31	0.14	0.99
0.4	70	32.50	95.68	22.35	84.70	99.08	0.32	0.14	0.99
0.7	70	20.91	60.85	14.32	53.13	62.71	0.32	0.15	0.99
0.2	30	29.45	82.73	18.54	72.91	85.38	0.32	0.15	0.99
0.4	30	15.91	44.39	10.38	39.20	45.81	0.32	0.15	0.99
0.7	30	10.03	27.90	6.55	24.60	28.78	0.32	0.15	0.99

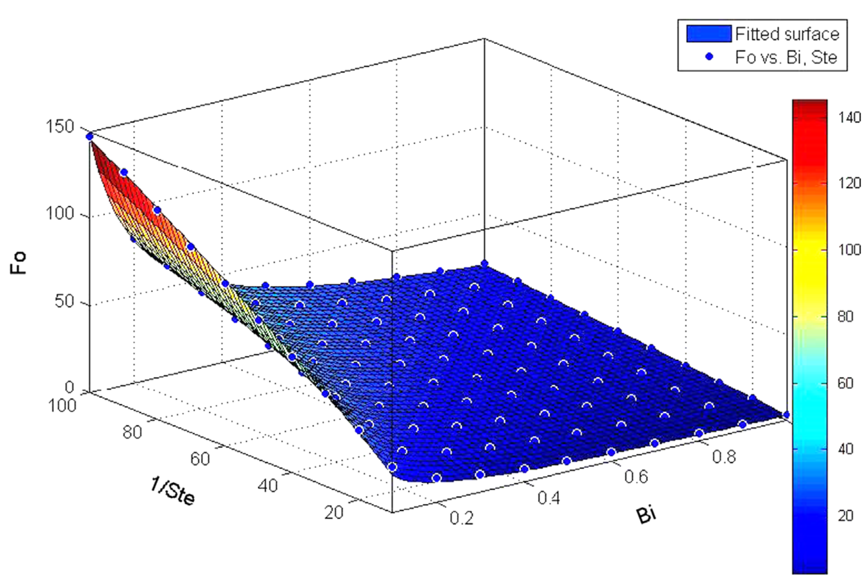


Fig. 9. Fitted surface shows the relationship between *Fo* of completely liquefied PCM wallboard VS (*Bi* and Ste^{-1}).

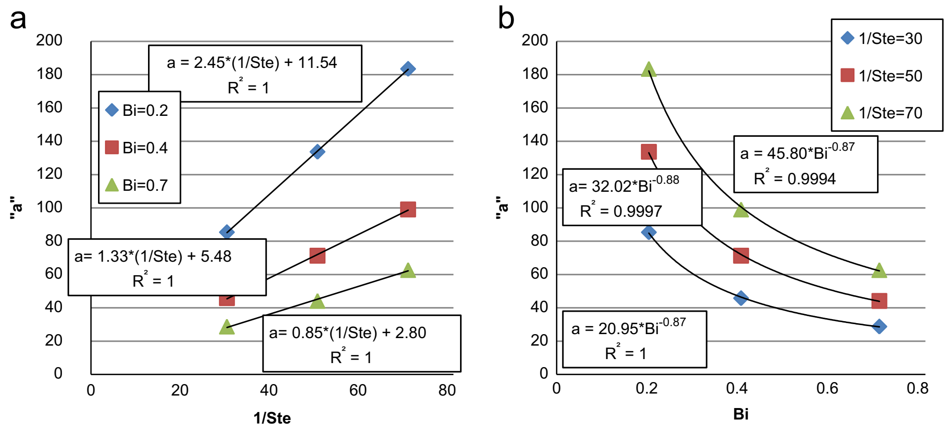


Fig. 11. The change of the peak of the fitted Gaussian function VS (a) $(Ste)^{-1}$ (b) *Bi*.

software [21]. The fitted surface is presented in Fig. 9. The surface fitted with *r*-square equal to 1 and its correlation is as follow;

$$Fo = 0.44 \times Bi^{-0.84} \times Ste^{-0.84} \tag{18}$$

To characterize the impact of the melting range, a number of simulations were conducted with three other melting ranges with different *Bi* and *Ste* numbers, in addition to the simulation scenarios explained before. The extra selected melting ranges are, (21–24) °C, (19–21) °C, and (20–24) °C. These ranges have been chosen in a way to be close to the room operational temperatures as recommended in previous researches [23,28,31]. The simulation scenarios for the impact of melting range consist of 27 new cases with Bi=(0.2, 0.4, or 0.7) and Ste^{-1}=(30, 50, or 70). Fig. 10 presents the effect of $\Psi = 1\ ^\circ C/(T_m - T_s)\ ^\circ C$ on the *Fo* number for completely liquefied PCM in different *Bi* and Ste^{-1} numbers. The graph shows that the relation between the *Fo* and Ψ follows the bell curve (Gaussian function). The Gaussian function is expressed as;

$$\text{Gaussian function}: \ y = f(x) = a \times \exp\left\{-\left[\frac{(x-b)}{c}\right]^2\right\} \tag{19}$$

The constant "*a*" is the height of the curve's peak, "*b*" is the position of the peak and "*c*" is the width of the curve. Fitting Gaussian function with each data set provides the constants of the fitted function in certain *Bi* and Ste^{-1} numbers. The measured *Fo* and the constants of the Gaussian functions are presented in Table 5.

As presented in Table 5, while the position of the peak and the width of the fitted Gaussian functions are almost the same for all *Bi* and Ste^{-1} combinations, the height of the peak is different in those fitted functions. The correlation between the height of the peak, "*a*", and the dimensionless numbers was investigated to extend the results to other *Bi* and *Ste* of the PCM wallboard. These correlations are presented in Fig. 11.

Like *Fo*, the peak height (*a*) is increasing linearly by increasing the Ste^{-1} number for a given *Bi* number. Moreover, the logarithmic magnitude of the peak height "*a*" is decreasing linearly with the logarithmic value of *Bi* number for a given *Ste* number.

Considering the melting range of a PCM wallboard as a design parameter, the study shows that the material has higher *Fo* of fully liquefied when its melting range is around 3–4 °C.

4. Conclusions

PCM wallboard can be applied to shift the peak load to the off-peak period. Either the thickness or the thermo-physical properties of the wallboard can be used as design parameter in order to properly find the charging time. In order to take advantage of the PCM's latent heat, it needs to be liquefied in a sufficient time to be utilized during peak period. Therefore, to select an appropriate PCM wallboard, a design tool needs to relate the PCM thickness and its thermo-physical properties to the charging time. The tool can be used either as a scale to select the appropriate thickness of the PCM wallboard or to modify its thermo-physical properties to satisfy the design objective.

In this study, the thermal dynamic of a PCM wallboard is characterized using the *Bi*, *Ste*, and *Fo* numbers. The relationships between *Fo* of a completely liquefied PCM and the other dimensionless numbers were identified. It was presented that the *Fo* is increasing linearly by decreasing the *Ste* number for a given *Bi* number. Moreover, increasing the *Bi* number of a PCM wallboard resulted in the reduction of *Fo* measured for fully melted PCM. In the next step, a new correlation between the *Fo* and both *Bi* and *Ste* numbers was developed. The developed correlation or the graphs can be employed to specify the appropriate design thickness of a PCM wallboard with its determined thermo-physical properties which can be charged in a sufficient time during off-peak period.

Moreover, in the case of some restrictions for the thickness of the wall or space limits, the correlation can be utilized to characterize the appropriate thermo-physical properties of a PCM wallboard with pre-determined thickness. Finally, the results of the effect of melting range conclude that a 2–3 °C range has the highest *Fo* of the completely liquefied PCM in a certain *Bi* and *Ste* numbers.

Acknowledgements

The authors would like to express their gratitude to the Public Works and Government Services Canada for their support.

References

[1] Ahmad M, Bontemps A, Sallée H, Quenard D. Experimental investigation and computer simulation of thermal behaviour of wallboards containing a phase change material. Energy Build 2006;38:357–66.
[2] Arkar C, Vidrih B, Medved S. Efficiency of free cooling using latent heat storage integrated into the ventilation system of a low energy building. Int J Refrig 2007;30:134–43, http://dx.doi.org/10.1016/j.ijrefrig.2006.03.009.
[3] Braun JE, Lee KH. Assessment of demand limiting using building thermal mass in small commercial buildings. ASHRAE Trans 2006;112:547–58.
[4] Dutil Y, Rousse DR, Salah NB, Lassue S, Zalewski L. A review on phase-change materials: mathematical modeling and simulations. Renewable Sustainable Energy Rev 2011;15:112–30.

[5] El-Sawi A, Haghighat F, Akbari H. Assessing long-term performance of centralized thermal energy storage system. Appl Therm Eng 2014;62:313–21, http://dx.doi.org/10.1016/j.applthermaleng.2013.09.047.
[6] Ettouney H, El-Dessouky H, Al-Kandari E. Heat transfer characteristics during melting and solidification of phase change energy storage process. Ind Eng Chem Res 2004;43:5350–7, http://dx.doi.org/10.1021/ie030495b.
[7] Ettouney H, El-Dessouky H, Al-Ali A. Heat transfer during phase change of paraffin wax stored in spherical shells. J Sol Energy Eng 2005;127:357–65.
[8] Farid MM, Khudhair AM, Razack SAK, Al-Hallaj S. A review on phase change energy storage: materials and applications. Energy Convers Manage 2004;45:1597–615.
[9] HydroQuebec. (2007) Demande R-3648-2007. Hydro Quebec Distribution-1.
[10] HydroQuebec. (2011) Demande R-3776-2011. Hydro Quebec Distribution-2.
[11] Johannes K, Virgone J. TASK C report of the Annex 23 of the International Energy Agency, applying energy storage in buildings of the future, prepared. CETHIL Thermal Center of Lyon School of Architecture; 2011.
[12] Khudhair AM, Farid MM. A review on energy conservation in building applications with thermal storage by latent heat using phase change materials. Energy Convers Manage 2004;45:263–75.
[13] Kuznik F, Virgone J, Noel J. Optimization of a phase change material wallboard for building use. Appl Therm Eng 2008;28:1291–8.
[14] Kuznik F, David D, Johannes K, Roux J-J. A review on phase change materials integrated in building walls. Renewable Sustainable Energy Rev 2011;15:379–91.
[15] Lee K-H, Braun JE. Evaluation of methods for determining demand-limiting setpoint trajectories in buildings using short-term measurements. Build Environ 2008;43:1769–83.
[16] Lee K-h, Braun JE. Development of methods for determining demand-limiting setpoint trajectories in buildings using short-term measurements. Build Environ 2008;43:1755–68.
[17] Li G. Review of thermal energy storage technologies and experimental investigation of adsorption thermal energy storage for residential application. Master thesis. University of Maryland at College Park (2013).
[18] Li G, Hwang Y, Radermacher R. Review of cold storage materials for air conditioning application. Int J Refrig 2012;35:2053–77, http://dx.doi.org/10.1016/j.ijrefrig.2012.06.003.
[19] Li G, Hwang Y, Radermacher R, Chun H-H. Review of cold storage materials for subzero applications. Energy 2013;51:1–17, http://dx.doi.org/10.1016/j.energy.2012.12.002.
[20] Lin K, Zhang Y, Xu X, Di H, Yang R, Qin P. Modeling and simulation of underfloor electric heating system with shape-stabilized PCM plates. Build Environ 2004;39:1427–34.
[21] Matlab. (2010) R2010b Math Work Documentation. Math Works Inc.
[22] Mirzaei PA, Haghighat F. Modeling of phase change materials for applications in whole building simulation. Renewable Sustainable Energy Rev 2012;16:5355–62, http://dx.doi.org/10.1016/j.rser.2012.04.053.
[23] Neeper DA. Thermal dynamics of wallboard with latent heat storage. Sol Energy 2000;68:393–403.
[24] Nkwetta DN, Haghighat F. Thermal energy storage with phase change material—a state-of-the art review. Sustainable Cities and Society. http://dx.doi.org/10.1016/j.scs.2013.05.007.
[25] Robert A, Kummert M. Designing net-zero energy buildings for the future climate, not for the past. Build Environ 2012;55:150–8, http://dx.doi.org/10.1016/j.buildenv.2011.12.014.
[26] The natural resources CANADA. (2008) Energy use data handbook tables (CANADA): Table 2. Online Available: ⟨http://oee.nrcan.gc.ca/corporate/statistics/neud/dpa/handbook_tables.cfm?⟩ ATTR=0 (Last Access 28 October 2011).
[27] Verma P, Varun Singal SK. Review of mathematical modeling on latent heat thermal energy storage systems using phase-change material. Renewable Sustainable Energy Rev 2008;12:999–1031.
[28] Xu X, Zhang Y, Lin K, Di H, Yang R. Modeling and simulation on the thermal performance of shape-stabilized phase change material floor used in passive solar buildings. Energy Build 2005;37:1084–91.
[29] Zalba B, Marín JM, Cabeza LF, Mehling H. Review on thermal energy storage with phase change: materials, heat transfer analysis and applications. Appl Therm Eng 2003;23:251–83.
[30] Zhang Y, Zhou G, Lin K, Zhang Q, Di H. Application of latent heat thermal energy storage in buildings: state-of-the-art and outlook. Build Environ 2007;42:2197–209.
[31] Zhou G, Zhang Y, Wang X, Lin K, Xiao W. An assessment of mixed type PCM-gypsum and shape-stabilized PCM plates in a building for passive solar heating. Sol Energy 2007;81:1351–60.